

Monitoring Bone Marrow-Originated Mesenchymal Stem Cell Traffic to Myocardial Infarction Sites Using Magnetic Resonance Imaging

Yidong Yang,^{1,2} Autumn Schumacher,¹ Yuhui Yang,¹ Jimei Liu,¹
Xingming Shi,³ William D. Hill,^{4,5} and Tom C.-C. Hu^{1,2*}

How stem cells promote myocardial repair in myocardial infarction (MI) is not well understood. The purpose of this study was to noninvasively monitor and quantify mesenchymal stem cells (MSC) from bone marrow to MI sites using magnetic resonance imaging (MRI). MSC were dual-labeled with an enhanced green fluorescent protein and micrometer-sized iron oxide particles prior to intra-bone marrow transplantation into the tibial medullary space of C57Bl/6 mice. Micrometer-sized iron oxide particles labeling caused signal attenuation in T_2^* -weighted MRI and thus allowed noninvasive cell tracking. Longitudinal MRI demonstrated MSC infiltration into MI sites over time. Fluorescence from both micrometer-sized iron oxide particles and enhanced green fluorescent protein in histology validated the presence of dual-labeled cells at MI sites. This study demonstrated that MSC traffic to MI sites can be noninvasively monitored in MRI by labeling cells with micrometer-sized iron oxide particles. The dual-labeled MSC at MI sites maintained their capability of proliferation and differentiation. The dual-labeling, intra-bone marrow transplantation, and MRI cell tracking provided a unique approach for investigating stem cells' roles in the post-MI healing process. This technique can potentially be applied to monitor possible effects on stem cell mobilization caused by given treatment strategies. Magn Reson Med 65:1430–1436, 2011. © 2011 Wiley-Liss, Inc.

Key words: murine model; myocardial infarction; mesenchymal stem cells; magnetic resonance imaging; fluorescent imaging

A major complication of myocardial infarction (MI) is heart failure (1), since the scar tissue healing over the necrosed myocardium contains no contractile or pacemaker myocytes (2). Stem cell-based therapies have been explored to potentially regenerate healthy tissue at MI

sites, given that the heart lacks the necessary cardiomyocyte progenitors to do so by itself (3). However, the roles of stem cells in the myocardial repair and remodeling processes are as yet unknown (4,5).

Cells such as embryonic stem cells (6), human embryonic stem cells-derived cardiomyocytes (7), skeletal myocytes (8), and bone marrow-derived stem cells (9,10) have been previously transplanted into infarcted myocardium. However, complications have occurred when applying these cells to myocardial repair, including adverse immunological response and/or teratoma formation (11), highly complex harvest process (12), and failure to functionally integrate with the host tissue (13). Compared with other cell types, mesenchymal stem cells (MSC) demonstrate advantages in cardiac cell therapy since they exhibit a multi-lineage plasticity, a reduced immune response, and an easy harvest process (14,15). Research by Quevedo et al. (16) showed that MSC were capable of restoring cardiac function with an increase of ejection fraction from $35.0 \pm 1.7\%$ to $41.3 \pm 2.7\%$ over 12 weeks in swine receiving transendocardial injection of 200 million MSC.

Previous studies attempted to improve cardiac structure and function by directly delivering labeled stem cells into the damaged myocardium. However, this method usually led to severe cell loss (12). Studies also showed that intracoronary and intravenous injections were no more successful than the intramyocardial route at rendering satisfactory graft efficiency (17–19). Furthermore, transfer of iron oxide particles from originally labeled cells to macrophages can lead to false interpretation of magnetic resonance imaging (MRI) data (20,21), which imposes additional disadvantage for intramyocardial delivery. Intra-bone marrow transplantation is an alternative delivery method, which has exhibited improved engraftment (22). The bone marrow milieu provides a native environment for transplanted cell engraftment and proliferation.

Therefore, the purpose of this study was to investigate MSC's infiltration traffic from the bone marrow to MI sites by an intra-bone marrow cell delivery method. MSC were labeled with enhanced green fluorescent protein (eGFP) and micrometer-sized iron oxide particles (MPIO), which were also tagged with a Suncoast Yellow fluorescent dye. MPIO labeling enabled the noninvasive cell tracking with MRI. Fluorescence from both eGFP and MPIO was used to confirm the MRI findings by histological fluorescent imaging. This study intended to demonstrate that combining intra-bone marrow cell delivery, dual-cell labeling, and MRI cell tracking is a

¹Department of Radiology, Small Animal Imaging, Medical College of Georgia, Augusta, Georgia, USA.

²Nuclear and Radiological Engineering and Medical Physics Program, George W. Woodruff School of Mechanical Engineering, Georgia Institute of Technology, Atlanta, Georgia, USA.

³Department of Pathology, Medical College of Georgia, Augusta, Georgia, USA.

⁴Department of Cellular Biology and Anatomy, Medical College of Georgia, Augusta, Georgia, USA.

⁵Veterans Affairs Medical Center, Medical College of Georgia, Augusta, Georgia, USA.

Grant sponsor: American Health Assistance Foundation (National Heart Foundation).

*Correspondence to: Tom C.-C. Hu, PhD, MBA, Medical College of Georgia, 1410 Laney Walker Blvd CN-3155, Augusta, GA 30912. E-mail: tom.cc.hu@gmail.com

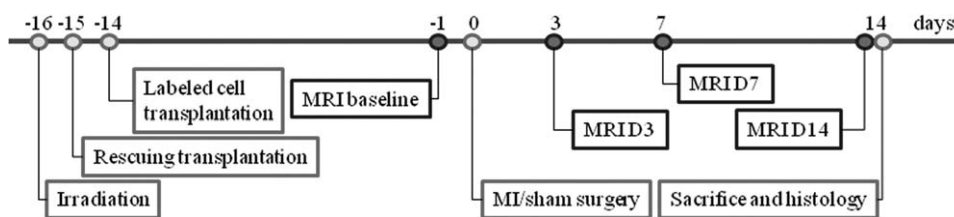
Received 12 April 2010; revised 1 October 2010; accepted 27 October 2010.

DOI 10.1002/mrm.22735

Published online 1 February 2011 in Wiley Online Library (wileyonlinelibrary.com).

© 2011 Wiley-Liss, Inc.

FIG. 1. Overall experiment time course. MI: myocardial infarction; MRI: magnetic resonance imaging.



promising methodology for studying stem cells mobilization in animal MI models.

MATERIALS AND METHODS

Overall Experimental Protocol

All animal procedures were performed in compliance with the Institutional Animal Care and Use Committee at the Medical College of Georgia, Augusta, GA. Adult male C57Bl/6 mice (6–12 weeks old, 23.8 ± 3.0 g) underwent irradiation, unlabeled rescuing bone marrow cell transplantation (1 day after irradiation), and transplantation of the labeled MSC (2 days after irradiation). At 14 days after labeled MSC transplantation, one animal group underwent MI surgery as an experimental group (Experimental group, $n = 7$); another group underwent sham-operated surgery (thoracotomy without any heart injury) as a sham control group (Sham control, $n = 7$). A third group receiving neither irradiation nor cell transplantation underwent MI surgery as MI control (MI control, $n = 6$). MRIs were performed on all mice at baseline, 3 days (D3), 7 days (D7), and 14 days (D14) post-MI or sham surgery. Figure 1 illustrates the overall experimental time course.

MSC Isolation and Culture

Bone marrow was harvested from 18-month-old C57Bl/6 mice by flushing the femora and tibiae with complete isolation medium consisting of RPMI-1640 with 9% heat-inactivated fetal bovine serum, 9% horse serum, 100 U/mL penicillin, 100 μ g/mL streptomycin, and 12 μ mol/L L-glutamine (23). The bone marrow was then dispersed into single-cell suspension and plated in flasks. To minimize MSC contamination with hematopoietic progenitor cells, the bone marrow cell suspension was allowed to adhere to the flasks for 3 hours at 37°C in a 5% CO₂ atmosphere (24). The media was then removed, the flask containing adherent cells gently washed with phosphate-buffered saline, and the cells cultured in complete isolation medium until they reached 80% confluence. Cells were then lifted by trypsin and subjected to negative immuno-selection by using magnetic beads to remove any hematopoietic lineage cells (25). The magnetic beads had been conjugated with CD11b, CD11c, CD45R/220B, and PDCA-1 monoclonal antibody. The hematopoietic lineage cells removed in this process included granulocytes, macrophages, myeloid-derived dendritic cells, natural killer cells, B lymphocytes, T lymphocytes, classical dendritic cells, plasmacytoid dendritic cells, and macrophage progenitors. Last, all cells negative for these antigens were subjected to a positive immuno-selection using stem cell

antigen-1 (Sca-1) monoclonal antibody conjugated magnetic beads.

MSC Labeling and Delivery

First, MSC were fluorescently labeled with eGFP via infecting the cells with retroviral vectors expressing eGFP (Δ U3-GFP) (26). The eGFP allowed cells to be visualized with fluorescent imaging. Next, the MSC were magnetically labeled with 1.63 μ m MPIO (Bangs Laboratories, Fishers, IN). MPIO have a polymer-coated magnetite core (42.5% weight) and are tagged with a Suncoast Yellow fluorescent dye. The magnetic core and Suncoast Yellow fluorescence allowed MPIO to be visualized via MR and fluorescent imaging, respectively. For labeling, MPIO were opsonized in 50% fetal bovine serum for 1 h at 37°C, washed in phosphate-buffered saline and resuspended in 1 mL expansion media with a concentration of 1×10^8 MPIO per mL. MSC were then incubated in 10 mL of media with a concentration of 1×10^6 MPIO per mL for 48 h.

Labeling outcomes were evaluated using a Zeiss Axiovert 10 microscope (Carl Zeiss, Jena, Germany) with a SPOT camera and software (Diagnostic Instruments, Sterling Heights, MI). The dual-labeled MSC were identified by the co-localization of eGFP and Suncoast Yellow fluorescence. Labeling efficiency was measured by randomly selecting labeled-cell cultures. The ratio of the number of dual-labeled cells to the total cell number was calculated within a single fluorescent image (20 \times magnification). MSC were further examined under an electron microscope to confirm MPIO were inside the cells. These dual-labeled cells maintained their capability of differentiation during a 10-day observation.

For the Experimental and Sham control groups, animals underwent irradiation with ¹³⁷Cs using a Gamma-cell 40 irradiator (Best Theratronics, Ottawa, ON, Canada). A dose of 8.0 Gy was used to ablate the bone marrow. The animals received a rescuing donation of unlabeled $\sim 0.5\text{--}2 \times 10^6$ bone marrow cells via retro-orbital plexus injection within 24 h after irradiation. Two days after the irradiation, each animal was properly anesthetized with a mixture of medical air, oxygen (1:1), and $\sim 2.0\%$ isoflurane (Abbott Laboratories, Abbott Park, IL), and a hole was drilled into the proximal articular surface with a 26-gauge needle. Approximately 30–50 μ L of bone marrow was then aspirated from the bone marrow cavity, and $\sim 6.6 \times 10^5$ eGFP and MPIO dual-labeled MSC (1.3 million cells per mL in phosphate-buffered saline) were transplanted into the tibial medullary space. The mice were allowed to recover in a postoperative recovery chamber under careful supervision before being returned to their cages.

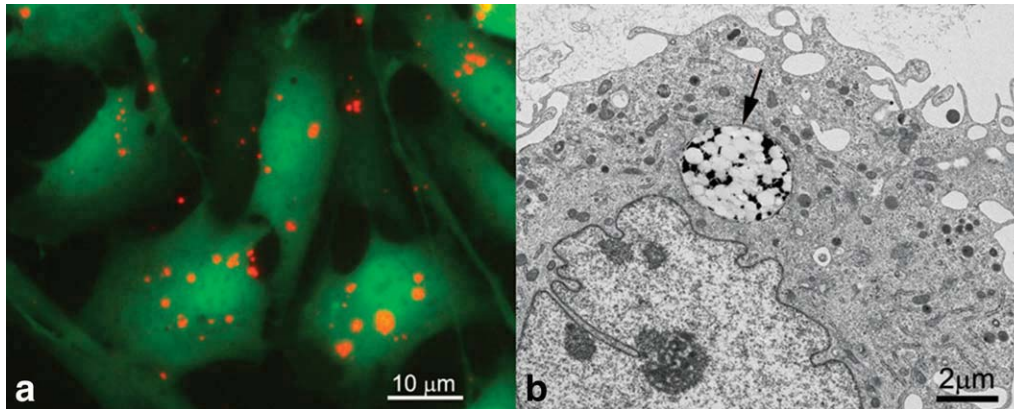


FIG. 2. Dual-labeled MSC with eGFP and MPIO. **a**: a merged fluorescent image of dual-labeled MSC. The eGFP expression is in green and MPIO are indicated by red spots. **b**: Image from an electron microscope showing MPIO engulfment inside a cell. The black arrow indicates a MPIO particle. [Color figure can be viewed in the online issue, which is available at wileyonlinelibrary.com.]

Myocardial Infarction and Magnetic Resonance Imaging

The MI and sham surgeries were performed 2 weeks after MSC transplantation using previously described procedures (27). Briefly, mice were anesthetized with an intraperitoneal injection of ketamine/xylazine at a dose of 2 μ L/g body weight. The Sham control mice had their chests immediately sutured after performing the thoracotomy without injuring the heart. The MI control mice had their left anterior descending coronary artery permanently ligated to produce an acute infarction in the left ventricular myocardium. The mice were then allowed to recover for 3 days before next MRI.

MRI procedures were conducted using a previously described protocol (27). Each mouse was anesthetized with a mixture of medical air, oxygen (1:1), and 1.5–2.0% isoflurane, maintaining a respiration rate of 61 ± 6 breaths per minute and a heart rate of 434 ± 58 beats per minute for all MRI sessions. MRI was performed on a horizontal 7.0-T, 21-cm MRI spectrometer (Bruker Instruments, Billerica, MA) equipped with a micro-imaging gradient insert (950 mT/m). A 35-mm inner diameter volume coil was used to transmit and receive signal at proton frequency (300 MHz). Short-axis cardiac images were acquired through the left ventricle perpendicular to the long axis of the heart using two pulse sequences: (1) an electrocardiogram-gated gradient echo sequence with flow compensation (GEFC) that acquired single T_2^* -weighted images, and (2) an electrocardiogram-gated GEFC cine sequence that acquired movies of cardiac movement during the cardiac cycle. The gradient echo sequence was sensitive enough to detect the signal attenuation generated by MPIO (28,29). The parameters for the GEFC sequence were: echo time/repetition time = 4/120 ms; flip angle = 30°; field of view = 30 \times 30 mm; slice thickness = 1 mm; matrix = 256 \times 256; and number of average = 8. Cardiac function such as left ventricular ejection fraction (LVEF) was monitored using the cine sequence. The parameters for GEFC cine sequence were: echo time/repetition time = 4/16 ms; flip angle = 25°; field of view = 30 \times 30 mm; slice thickness = 1 mm; matrix = 128 \times 128; number of average = 8; and eight frames in one cardiac cycle.

LVEF was calculated using the left ventricular end-diastolic volume (LVEDV) and left ventricular end-systolic volume (LVESV) determined from the endocardial contours in the end-diastolic and end-systolic phases, respectively [$LVEF(\%) = (LVEDV - LVESV)/LVEDV$]. Contrast-to-noise ratio (CNR) at the MI site was calculated using signal intensity (SI) measurements in the GEFC T_2^* -weighted images [$CNR = (SI_{MI} - SI_{norm})/SI_{bkg}$]. The SI_{MI} represented the SI at the MI region located where the left ventricular wall thinned; the MI region was confirmed by the akinetic contractility area seen in the cine images. The SI_{norm} represented the SI in the normal (noninfarcted) myocardium and the SI_{bkg} represented the background noise.

Histology

After completing the final MRI session and while still anesthetized, each animal was sacrificed by perfusing the body with 4% paraformaldehyde injected into the inferior vena cava. Once the blood was flushed out, the heart was removed from the body. After 2 days in paraformaldehyde, the heart was immersed in 30% sucrose and then sectioned into 10 μ m-thick transverse slices along the longitudinal axis. These tissue slices were then immuno-labeled with antibodies against fibroblast marker ER-TR7, macrophage/monocyte marker F4/80 and CD11. All slices were examined under a confocal microscope (Zeiss LSM 510 laser scanning microscope; Carl Zeiss, Jena, Germany) for fluorescent imaging.

Statistical Analysis

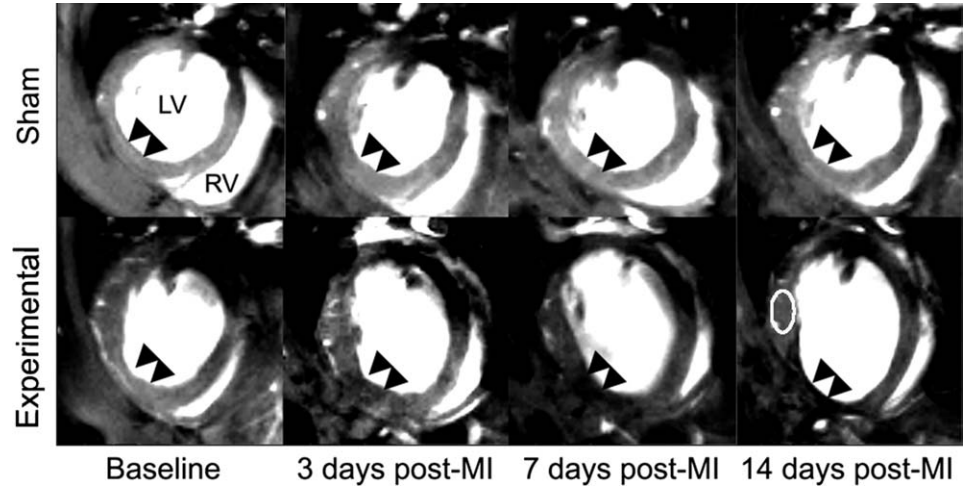
All data were presented as mean \pm standard error of mean. A two-way repeated-measures analysis of variance was used to compare differences in CNR and LVEF values between different groups followed by Bonferroni post hoc tests. The GraphPad Prism 5.01 (GraphPad Software Inc., San Diego, CA) was used for all statistical analyses with a significance level of 0.05.

RESULTS

MSC Labeling

Figure 2 demonstrates the dual-labeled MSC. Figure 2a shows the co-localization of eGFP and MPIO in these

FIG. 3. T_2^* -weighted short-axis cardiac MR images. Gradual signal attenuation was observed at MI sites for the Experimental group, suggesting labeled cells accumulation. No remarkable signal attenuation was observed for sham group. Arrows indicate MI sites or corresponding sites. The eclipse demonstrates the region of interest drawn in the normal myocardium used to calculate SI_{norm} . MI: myocardial infarction. LV: left ventricle. RV: right ventricle.



cells with the eGFP expression shown in green and MPIO represented by red spots. Figure 2b is an image from an electron microscopy confirming that MPIO were incorporated into the MSC. Based on 10 random measurements ($n = 10$), a labeling efficiency of $97.2 \pm 1.5\%$ was obtained for MPIO cell labeling.

MRI Cell Tracking

Figure 3 shows an example of longitudinal T_2^* -weighted MR images acquired to monitor labeled MSC infiltration into the MI sites. Gradual signal attenuation was observed in infarction sites over time for the Experimental group. No remarkable attenuation was observed at the corresponding sites for the Sham control mouse. Low SI localized in the posterior left ventricular wall was presumably artifacts caused primarily by cardiac motion.

Temporal infiltration of MPIO-labeled MSC at the MI site was quantified using CNR (Fig. 4a). The negative CNR values seen for the Experimental group represents signal attenuation around the MI sites indicative of MPIO-labeled cell infiltration. The continuous CNR attenuation over time denotes an increased MPIO-labeled

cell infiltration into the infarction site, which was not observed in either the Sham or MI control group. Two-way repeated measures analysis of variance test showed significant difference in CNR among all groups ($p < 0.0001$). As expected, no significant difference in CNR were found between any two groups at baseline ($p > 0.05$). Significant differences in CNR were found between the experimental group and Sham control group at 3 days ($p < 0.01$), 7 days ($p < 0.001$), and 14 days ($p < 0.001$) post-MI, and between the experimental group and MI control group at 7 days ($p < 0.05$) and 14 days ($p < 0.001$). The CNR differences between the Sham and MI control group were not significant at 7 days and 14 days ($p > 0.05$). The post-MI CNR attenuation for the MI control group was presumably caused by unintended hemorrhage during the surgical formation of the MI. The pronounced signal attenuation for the Experimental group indicates that the MPIO-labeled cells mobilized into the MI site from bone marrow and was successfully monitored with the T_2^* -weighted MRI technique. A considerable number of labeled cells also infiltrated into the border region adjacent to the MI site, causing signal attenuation in MRI. Part of the chest wall was

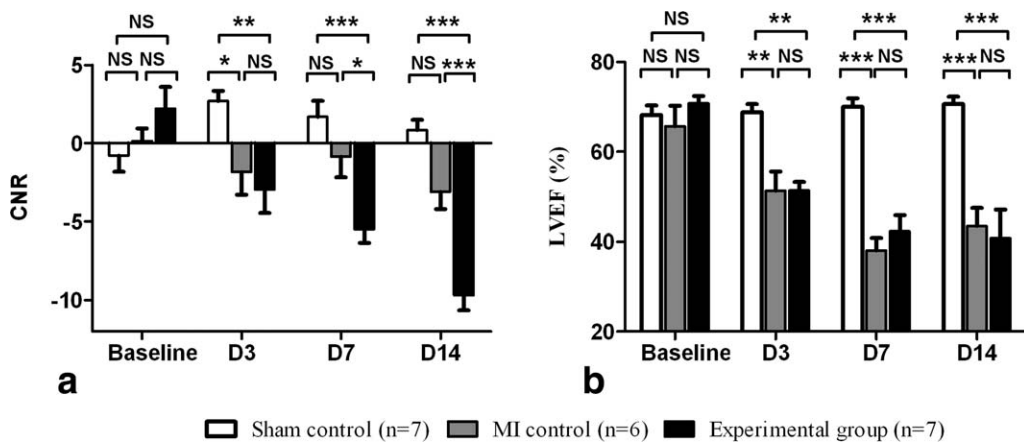


FIG. 4. CNR and LVEF. **a:** Continuous CNR attenuation for the Experimental group suggests labeled MSC infiltration into MI sites. **b:** Decrease in LVEF for both the experimental and MI control group evidences MI-caused cardiac dysfunction. NS: not significant; * $p < 0.05$; ** $p < 0.01$; *** $p < 0.001$. CNR: contrast-to-noise ratio; LVEF: left ventricular ejection fraction.

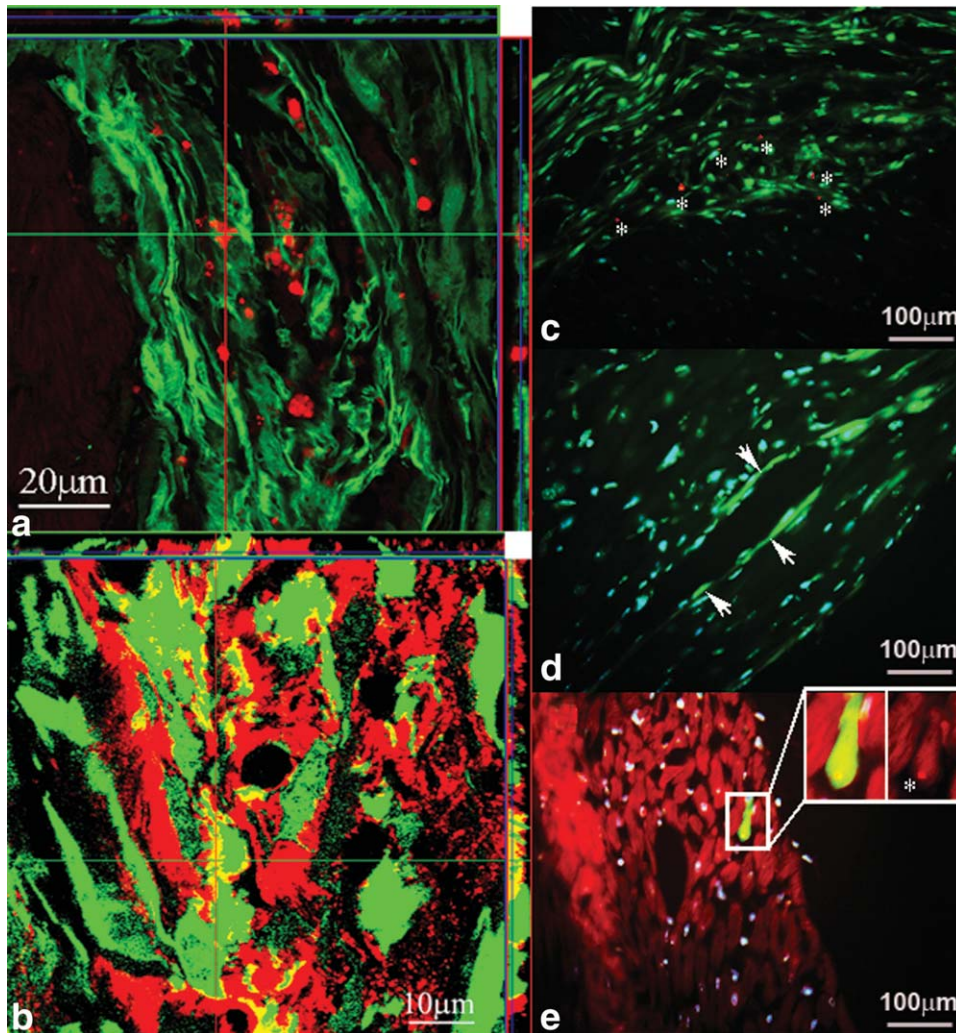


FIG. 5. Histological fluorescent images. **a:** Dual-labeled MSC contained both eGFP (green color) and MPIO particles (red spots). **b:** eGFP+ MSC and/or derivatives (green color) were positive to ER-TR7 antibody, a fibroblast marker (red color). Overlap of ER-TR7 and eGFP turned out to be yellow. **c:** The eGFP+ cells at the MI site had a fibroblast-like phenotype and a subset contain MPIO particles (red spots marked by asterisks). **d:** Some MSC-derived cells (marked by white arrows) lined the blood vessels. **e:** a cardiomyocyte-like MSC derivative inserted between the resident cardiomyocytes. The higher magnification insets show this eGFP+ cell also carried a MPIO particle (marked by the asterisk).

occasionally darkened due to the open-chest procedure which triggered the mobilization of labeled MSC homing to the injured site. Darkness at the left ventricular posterior wall was observed for most animals, which was potentially caused by motion artifact and/or iron deposition at the vicinity from the liver or lung.

LVEF was evaluated as a representation of cardiac performance (Fig. 4b). As expected, LVEF decreased following the MI surgery and gradually stabilized after 7 days for both the Experimental and MI control group. Two-way repeated measures analysis of variance test showed significant difference in LVEF among all groups ($p < 0.0001$). No significant difference in LVEF was found between any two groups at baseline ($p > 0.05$). Significant differences in the LVEF were found between the Sham group and both the MI control and Experimental group at 3 days ($p < 0.01$), 7 days ($p < 0.001$), and 14 days ($p < 0.001$) post-MI. No significant difference was found between the experimental group and MI control group at any time point ($p > 0.05$).

Histological Fluorescent Imaging

Fluorescent confocal imaging provided a three-dimensional view of the histology slices. Therefore this method

is well suited to examine the co-localization of dual labels. Figure 5a illustrated dual-labeled MSC at the MI site, with eGFP labeling identified by the green color and MPIO labeling by the red spots. This finding confirmed that dual-labeled MSC mobilized from the bone marrow into the MI site, thus validating MRI findings. Figure 5b shows that a subset of eGFP labeled MSC were also positive for ER-TR7 (i.e., the fibroblast biomarker). This merged image shows ER-TR7 expression in red and eGFP in green. The overlap between ER-TR7 and eGFP turned the color yellow, suggesting that a population of transplanted MSC differentiated into fibroblasts at the MI site. Figure 5c further shows many MSC derivatives at the MI site had a fibroblast-like phenotype and a subset contain MPIO particles. In Fig. 5d, some MSC-derived cells lined the blood vessels, indicating that MSC may contribute to the post-MI vascularization. Figure 5e shows a dual-labeled cardiomyocyte-like MSC derivative inserting in between the resident cardiomyocytes. These histological findings confirmed that the dual-labeled MSC maintained their capability of proliferating, migrating and differentiating following intra-bone marrow transplantation. Additional immunohistological staining with F4/80 and CD11b antibodies, two macrophage biomarkers, demonstrated no macrophages with MPIO particles.

DISCUSSION

This study demonstrated how combining the *in vivo* MRI and *ex vivo* fluorescent imaging techniques assessed the temporal characteristics of MSC homing to MI sites following their intra-bone marrow transplantation. The main purpose of this study was to investigate a new methodology for studying the roles of stem cells *in vivo*. The experimental group received irradiation, rescue cell transplantation, and labeled cell transplantation. Radiation ablated the stem cells in the bone marrow of the experimental group to create a niche for later transplanted labeled MSC engraftment. The reason for initial engraftment of the labeled MSC into the bone marrow was to examine the MI activation process which triggered the release of labeled MSC from its native environment. Dual labeling of MSC with eGFP and MPIO allowed non-invasively and temporally tracking MSC infiltration into the MI sites, as well as histological confirmation of the MRI findings. This dual labeling strategy with both GFP and iron oxide particles has been studied previously (30–32). MRI data illustrated the post-MI attenuation of CNR over time, indicating that mediation of MSC in myocardial remodeling lasted at least 2 weeks. MRI findings were confirmed by histological fluorescent imaging, in which many dual-labeled cells were observed around MI sites. However, correlating the counts/density of labeled cells in histology with the SI in MRI at the MI site shall further consolidate the findings.

The intra-bone marrow transplantation technique provided a unique cell delivery method for studying bone marrow-originated stem cells in post-MI animal models, since the bone marrow provides a native environment for implanted cells to survive and proliferate. This study showed that dual-labeled MSC maintained their capability of migrating and differentiating following intra-bone marrow transplantation. Once irradiation prepared the bone marrow for MSC engraftment, the 2-week span between the transplantation and sham/MI surgeries proved to be an adequate amount of time for this cell engraftment to occur. The potential pathway of the labeled MSC from bone marrow to the infarction site is through the blood circulating in either survived vessels, regenerated collateral vessels, or neovasculatures. Indeed, we observed MSC or their derivatives lining the blood vessels. However, the exact mechanisms of labeled cell homing, engraftment, as well as the engraftment efficiency are as yet unknown and necessitate further intensive investigation.

At the MI site, MSC have the potential to differentiate into different cell types (33). Previous research found that MSC were able to differentiate into vascular smooth muscle cells, endothelial cells, and even cardiomyocytes (16). In this study, MSC-derived fibroblasts were found around the MI site, which potentially contribute to scar formation. It was also observed that MSC derivatives lined the blood vessel structures, potentially contributing to angiogenesis. Interestingly, it was observed that some dual-labeled cardiomyocyte-like cells were inserted between the host myocardial cells based on cell morphology. However, it warrants further investigation to confirm that those transplanted cells are able to differen-

tiate into cardiomyocytes (e.g., by using cardiomyocyte-specific staining to confirm some dual-labeled cells are cardiomyocytes). Further experiments are warranted to elucidate the capability of MSC differentiation and its function during the MI process.

MPIO were used in this study as cell labeling to provide image contrast by causing signal loss at the MI site. Currently, many types of MR cell labeling probes are being used or under investigation. Of these probes, iron oxide particles cause negative contrast by producing dark signal (28,34); gadolinium or manganese-based agents cause positive contrast by increasing SI (35,36). However, interpretation of the signal alteration caused by these probes is complicated due to the addition of artifacts in tissue background, such as hemorrhage or tissue interface. Novel MR agents that are not based on ^1H signal alteration are in development, with which image contrast will be less affected by tissue artifacts (37,38). MR spectroscopy can also be potentially used as a means to quantify cells labeled with either ^1H or non- ^1H based contrast agents. In the future study, the infarction area can be outlined by using gadolinium-based contrast agent to enhance the MR signal *in situ*. It is also possible to examine potential perfusion/flow effects in the infarct heart caused by labeled MSC infiltration with gadolinium-based contrast agent.

In conclusion, this study applied a dual labeling approach to monitor bone marrow-originated MSC traffic to MI sites. MPIO labeling produced a hypointensity in MR images and enabled noninvasive and temporal cell tracking. The fluorescent labeling allowed for *ex vivo* examination of labeled cells to confirm MRI findings. This technique with dual-labeling, bone marrow transplantation, and multiple imaging modalities provides a unique approach to investigate bone-marrow originated stem cells in cardiac remodeling. Once the dual-labeled cells infiltrated into the infarct heart, they maintained their ability to divide and differentiate and would contribute to healing process. In this manner, signaling pathways for tissue repair by stem cells can be tested and alteration in cell infiltration flux can be monitored. In the future, some experiments can be designed to investigate any cardiac function recovery caused by enhanced MSC infiltration, for instance, through modulation of the number of MSC homing to the MI site by using drugs such as granulocyte-colony stimulating factor that can facilitate MSC mobilization. Therefore, this technique has a potential application of monitoring treatment effects on cell mobilization and infiltration at diseased sites in drug development or post-treatment evaluation process.

REFERENCES

1. Velagaleti RS, Pencina MJ, Murabito JM, Wang TJ, Parikh NI, D'Agostino RB, Levy D, Kannel WB, Vasan RS. Long-term trends in the incidence of heart failure after myocardial infarction. *Circulation* 2008; 118:2057–2062.
2. Opie L. Heart physiology: from cell to circulation, 4th ed. Philadelphia: Lippincott Williams & Wilkins; 2004.
3. Li SC, Wang L, Jiang H, Acevedo J, Chang AC, Loudon WG. Stem cell engineering for treatment of heart diseases: potentials and challenges. *Cell Biol Int* 2009; 33:255–267.
4. Murry CE, Field LJ, Menasche P. Cell-based cardiac repair: reflections at the 10-year point. *Circulation* 2005; 112:3174–3183.

5. Menasche P. Cell-based therapy for heart disease: a clinically oriented perspective. *Mol Ther* 2009;17:758–766.
6. Yang L, Soonpaa MH, Adler ED, Roepke TK, Kattman SJ, Kennedy M, Henckaerts E, Bonham K, Abbott GW, Linden RM, Field LJ, Keller GM. Human cardiovascular progenitor cells develop from a KDR+ embryonic-stem-cell-derived population. *Nature* 2008;453:524–528.
7. Kehat I, Khimovich L, Caspi O, Gepstein A, Shofti R, Arbel G, Huber I, Satin J, Itskovitz-Eldor J, Gepstein L. Electromechanical integration of cardiomyocytes derived from human embryonic stem cells. *Nat Biotechnol* 2004;22:1282–1289.
8. Menasche P. Skeletal myoblasts for cardiac repair: act II? *J Am Coll Cardiol* 2008;52:1881–1883.
9. Carr CA, Stuckey DJ, Tatton L, Tyler DJ, Hale SJ, Sweeney D, Schneider JE, Martin-Rendon E, Radda GK, Harding SE, Watt SM, Clarke K. Bone marrow-derived stromal cells home to and remain in the infarcted rat heart but fail to improve function: an in vivo cine-MRI study. *Am J Physiol Heart Circ Physiol* 2008;295:H533–H542.
10. Shyu KG, Wang BW, Hung HF, Chang CC, Shih DT. Mesenchymal stem cells are superior to angiogenic growth factor genes for improving myocardial performance in the mouse model of acute myocardial infarction. *J Biomed Sci* 2006;13:47–58.
11. Nussbaum J, Minami E, Laflamme MA, Virag JA, Ware CB, Masino A, Muskheli V, Pabon L, Reinecke H, Murry CE. Transplantation of undifferentiated murine embryonic stem cells in the heart: teratoma formation and immune response. *FASEB J* 2007;21:1345–1357.
12. Laflamme MA, Chen KY, Naumova AV, Muskheli V, Fugate JA, Dupras SK, Reinecke H, Xu C, Hassanipour M, Police S, O'sullivan C, Collins L, Chen Y, Minami E, Gill EA, Ueno S, Yuan C, Gold J, Murry CE. Cardiomyocytes derived from human embryonic stem cells in pro-survival factors enhance function of infarcted rat hearts. *Nat Biotechnol* 2007;25:1015–1024.
13. Leobon B, Garcin I, Menasche P, Vilquin JT, Audinat E, Charpak S. Myoblasts transplanted into rat infarcted myocardium are functionally isolated from their host. *Proc Natl Acad Sci USA* 2003;100:7808–7811.
14. Pittenger MF, Mackay AM, Beck SC, Jaiswal RK, Douglas R, Mosca JD, Moorman MA, Simonetti DW, Craig S, Marshak DR. Multilineage potential of adult human mesenchymal stem cells. *Science* 1999;284:143–147.
15. Kawada H, Fujita J, Kinjo K, Matsuzaki Y, Tsuma M, Miyatake H, Muguruma Y, Tsuboi K, Itabashi Y, Ikeda Y, Ogawa S, Okano H, Hotta T, Ando K, Fukuda K. Nonhematopoietic mesenchymal stem cells can be mobilized and differentiate into cardiomyocytes after myocardial infarction. *Blood* 2004;104:3581–3587.
16. Quevedo HC, Hatzistergos KE, Oskoueï BN, Feigenbaum GS, Rodriguez JE, Valdes D, Pattany PM, Zambrano JP, Hu Q, McNiece I, Heldman AW, Hare JM. Allogeneic mesenchymal stem cells restore cardiac function in chronic ischemic cardiomyopathy via trilineage differentiating capacity. *Proc Natl Acad Sci USA* 2009;106:14022–14027.
17. Freyman T, Polin G, Osman H, Crary J, Lu M, Cheng L, Palasis M, Wilensky RL. A quantitative, randomized study evaluating three methods of mesenchymal stem cell delivery following myocardial infarction. *Eur Heart J* 2006;27:1114–1122.
18. Barbash IM, Chouraqui P, Baron J, Feinberg MS, Etzion S, Tessone A, Miller L, Guetta E, Zipori D, Kedes LH, Kloner RA, Leor J. Systemic delivery of bone marrow-derived mesenchymal stem cells to the infarcted myocardium: feasibility, cell migration, and body distribution. *Circulation* 2003;108:863–868.
19. Wei H, Ooi TH, Tan G, Lim SY, Qian L, Wong P, Shim W. Cell delivery and tracking in post-myocardial infarction cardiac stem cell therapy: an introduction for clinical researchers. *Heart Fail Rev* 2009;15:1–14.
20. Amsalem Y, Mardor Y, Feinberg MS, Landa N, Miller L, Daniels D, Ocherashvilli A, Holbova R, Yosef O, Barbash IM, Leor J. Iron-oxide labeling and outcome of transplanted mesenchymal stem cells in the infarcted myocardium. *Circulation* 2007;116(Suppl 11):I38–I45.
21. Qiao H, Zhang H, Zheng Y, Ponde DE, Shen D, Gao F, Bakken AB, Schmitz A, Kung HF, Ferrari VA, Zhou R. Embryonic stem cell grafting in normal and infarcted myocardium: serial assessment with MR imaging and PET dual detection. *Radiology* 2009;250:821–829.
22. Kushida T, Inaba M, Hisha H, Ichioka N, Esumi T, Ogawa R, Iida H, Ikehara S. Intra-bone marrow injection of allogeneic bone marrow cells: a powerful new strategy for treatment of intractable autoimmune diseases in MRL/lpr mice. *Blood* 2001;97:3292–3299.
23. Peister A, Mellad JA, Larson BL, Hall BM, Gibson LF, Prockop DJ. Adult stem cells from bone marrow (MSCs) isolated from different strains of inbred mice vary in surface epitopes, rates of proliferation, and differentiation potential. *Blood* 2004;103:1662–1668.
24. Gimble JM, Robinson CE, Wu X, Kelly N, Rodriguez BR, Kliever SA, Lehmann JM, Morris DC. Peroxisome proliferator-activated receptor-gamma activation by thiazolidinediones induces adipogenesis in bone marrow stromal cells. *Mol Pharmacol* 1996;50:1087–1094.
25. Tropel P, Noel D, Pladet N, Legrand P, Benabid AL, Berger F. Isolation and characterisation of mesenchymal stem cells from adult mouse bone marrow. *Exp Cell Res* 2004;295:395–406.
26. Yang N, Zhang W, Shi X. Glucocorticoid-induced leucine zipper (GILZ) mediates glucocorticoid action and inhibits inflammatory cytokine-induced COX-2 expression. *J Cell Biochem* 2008;103:1671–1680.
27. Yang Y, Yang Y, Yanasak N, Schumacher A, Hu TC. Temporal and noninvasive monitoring of inflammatory-cell infiltration to myocardial infarction sites using micrometer-sized iron oxide particles. *Magn Reson Med* 2010;63:33–40.
28. Shapiro EM, Skrtic S, Koretsky AP. Sizing it up: cellular MRI using micron-sized iron oxide particles. *Magn Reson Med* 2005;53:329–338.
29. Shapiro EM, Skrtic S, Sharer K, Hill JM, Dunbar CE, Koretsky AP. MRI detection of single particles for cellular imaging. *Proc Natl Acad Sci USA* 2004;101:10901–10906.
30. Yano S, Kuroda S, Shichinohe H, Hida K, Iwasaki Y. Do bone marrow stromal cells proliferate after transplantation into mice cerebral infarct?—a double labeling study. *Brain Res* 2005;1065:60–67.
31. Moore A, Marecos E, Bogdanov A Jr, Weissleder R. Tumoral distribution of long-circulating dextran-coated iron oxide nanoparticles in a rodent model. *Radiology* 2000;214:568–574.
32. Zhang Z, Dharmakumar R, Mascheri N, Fan Z, Wu S, Li D. Comparison of superparamagnetic and ultrasmall superparamagnetic iron oxide cell labeling for tracking green fluorescent protein gene marker with negative and positive contrast magnetic resonance imaging. *Mol Imaging* 2009;8:148–155.
33. Pittenger MF, Mackay AM, Beck SC, Jaiswal RK, Douglas R, Mosca JD, Moorman MA, Simonetti DW, Craig S, Marshak DR. Multilineage potential of adult human mesenchymal stem cells. *Science* 1999;284:143–147.
34. Wang YX, Hussain SM, Krestin GP. Superparamagnetic iron oxide contrast agents: physicochemical characteristics and applications in MR imaging. *Eur Radiol* 2001;11:2319–2331.
35. Bellin MF. MR contrast agents, the old and the new. *Eur J Radiol* 2006;60:314–323.
36. Strijkers GJ, Mulder WJ, van Tilborg GA, Nicolay K. MRI contrast agents: current status and future perspectives. *Anticancer Agents Med Chem* 2007;7:291–305.
37. Srinivas M, Heerschap A, Ahrens ET, Figdor CG, de Vries IJ. (19)F MRI for quantitative in vivo cell tracking. *Trends Biotechnol* 2010;28:363–370.
38. Bonetto F, Srinivas M, Heerschap A, Mailliard R, Ahrens ET, Figdor CG, de Vries IJ. A Novel (19)F agent for detection and quantification of human dendritic cells using magnetic resonance imaging. *Int J Cancer*. Epub ahead of print. DOI: 10.1002/ijc.25672.